PRAMANA
— journal of
physics

Vol. 66, No. 1
January 2006
pp. 113–129

Vortex phase diagram studies in the weakly pinned single crystals of YNi_2B_2C and $LuNi_2B_2C$

D JAISWAL-NAGAR[1,*], D PAL[2], M R ESKILDSEN[2], P C CANFIELD[3], H TAKEYA[4], S RAMAKRISHNAN[1] and A K GROVER[1,†]

[1]Department of Condensed Matter Physics and Materials Science, Tata Institute of Fundamental Research, Homi Bhabha Road, Colaba, Mumbai 400 005, India

[2]Department of Physics, University of Notre Dame, Notre Dame, IN 46556, USA

[3]Ames Laboratory, Iowa State University, Ames, Iowa, 50011, USA

[4]National Institute for Materials Science, 3-13, Sakura, Tsukuba, Ibakari, 305003, Japan

E-mail: *shikha@tifr.res.in; †grover@tifr.res.in

Abstract. We present a study of magnetization measurements performed on the single crystals of YNi_2B_2C and $LuNi_2B_2C$. For both the compounds, we find flux jumps in magnetisation values in the respective field regions, where the structural transitions in the flux line lattice symmetry have been reported in these systems via the small angle neutron scattering experiments. The magnetisation hysteresis loops and the AC susceptibility measurements show pronounced peak effect as well as second magnetisation peak anomaly for both YNi_2B_2C and $LuNi_2B_2C$. Based on these results, a vortex phase diagram has been constructed for YNi_2B_2C for $H\|c$ depicting different glassy phases of the vortex matter.

Keywords. Flux jumps; peak effect; second magnetisation peak; YNi_2B_2C; $LuNi_2B_2C$; vortex phase diagram.

PACS Nos 74.25.Qt; 74.70.Dd

1. Introduction

Type II superconductivity in the presence of magnetic field (**B**) is characterized by the creation of a vortex lattice, which comprises flux lines in a regular (e.g., hexagonal) arrangement. A quantum of flux (in units of $hc/2e$) associates with each flux line. In an ideal defect-free system, a perfect hexagonal flux line lattice does not sustain any critical current as it moves under the influence of a Lorentz force ($\mathbf{J} \times \mathbf{B}$). Presence of even point disorder in the atomic lattice can change this situation considerably, and the superconductor can start carrying a finite critical current density (J_c). The J_c is a material property attributable to the pinning effects arising from the preferential location of the cores of the flux lines near statistical fluctuation in the defect density and/or the atomic inhomogeneities. With the increase in field/temperature (H/T), J_c is expected to monotonically decrease. A sudden increase in J_c with the increase in H/T is therefore considered unusual.

An anomalous increase in J_c while approaching the normal/superconductor phase boundary is termed as the peak effect (PE) phenomenon [1], which has been a topic of intense research over the past few decades. A heuristic explanation of the PE given by Pippard [2] suggests that the shear modulus of the flux line lattice can collapse faster than the pinning force as the applied field approaches the upper critical field H_{c2}. Such a softened lattice can get more easily deformed and, hence, require more threshold force to dislodge the vortices from the pinning sites. Larkin and Ovchinnikov (LO) [3] have given a phenomenological theory which enunciates the notion of a Larkin domain [4] with a correlation volume V_c ($=R_c^2 L_c$), within which the flux lines are collectively pinned and the FLL can be considered to be quasi-ordered. According to the LO theory, J_c is inversely proportional to the square root of V_c. An anomalous increase in J_c, therefore, implies a reduction in the correlation volume V_c [5]. The PE thus marks a transition from an ordered flux line lattice to a disordered vortex state.

Apart from the PE anomaly, another anomalous feature in the magnetisation hysterisis loops is easily evident in the context of weakly pinned samples of high-temperature superconductors. This anomaly is seen deep inside the mixed state of high T_c cuprates and is termed as the second magnetisation peak (SMP) or the fish-tail effect, as the M–H hysteresis curve resembles the shape of a fish tail [6–8]. There have been assertions made that the SMP anomaly characterises some specific attributes of the high-temperature superconductors. Presence of a SMP anomaly distinct from the PE in samples of a conventional low-temperature superconductor along with that of a cuprate superconductor therefore aroused curiosity [9–12].

The quaternary borocarbide superconductors discovered about a decade ago [13,14] are very exciting systems [15], as they show interesting attributes, like, the co-existence of superconductivity and magnetism [16,17], unusual gap symmetry in their superconducting order parameter [18,19], abrupt transformation in the nearest-neighbour arrangement of the flux lines at low fields [20–24], presence of an order–disorder transformation in the FLL correlations *a la* PE at high fields, etc. [20,25–27]. The novel characteristic of the change in the local symmetry of the flux line lattice from square to rhombohedral (R1) and rhombohedral R1 to rhombohedral R2 (with abrupt change in the apex angle) has been extensively investigated in small angle neutron scattering (SANS) measurements [20–24]. Kogan *et al* [28] have advanced an explanation of the observed transitions at low fields by invoking the notion that the relationship between the supercurrent **j** and the magnetic vector potential **A** is non-local. In YNi_2B_2C crystals, the changes in the local symmetry of FLL have been observed at field values ≈100 mT [20–22], whereas, in the crystals of $LuNi_2B_2C$, similar transformations have been reported to occur in the field range of 20 to 50 mT [24].

The peak effect phenomenon in YNi_2B_2C and $LuNi_2B_2C$ crystals has also been explored via magnetisation and transport measurements in the recent past [20,25–27,29] by several workers. In one of the initial reports [29], PE is not clearly evident in the magnetisation hysteresis plots for $H \| c$ in YNi_2B_2C samples in the temperature range 3 K to 13 K. However, in a later study, the presence of the PE bubble in the M–H loops has been reported in the temperature range 5 K to 11 K in a better quality crystal of YNi_2B_2C for $H \| c$ [25]. In some other studies also [26,27], the presence of PE in magnetisation hysteresis data in a crystal of YNi_2B_2C has

been noted between 3 K and 11 K for $H\|c$. The transport measurements performed along with the small angle neutron scattering experiments in $LuNi_2B_2C$ crystals of the same batch [20] in the field-cooled states ($H\|c$) at 2.2 K also revealed the presence of the peak effect prior to the H_{c2} value.

We are presenting here some glimpses of the magnetisation studies carried out on the single crystals of the borocarbide superconductors, YNi_2B_2C and $LuNi_2B_2C$, with a view to sketch a vortex phase diagram in them. The YNi_2B_2C crystals chosen for the present work have been used earlier for the dHvA studies at very low temperatures (<1.4 K) and the $LuNi_2B_2C$ crystals have been selected from a batch grown for SANS experiments [15]. In both sets of crystals of the two compounds, the PE phenomenon is evident down to low fields (∼few mT) and high temperatures (few degrees below $T_c(0)$), attesting to their high purity.

2. Experimental details

A single crystal of YNi_2B_2C was obtained from a rod grown by traveling solvent floating zone method [30]. The single crystals of $LuNi_2B_2C$ were grown by flux method with Ni_2B as flux [15]. The YNi_2B_2C sample has $T_c(0) \approx 15.1$ K and H_{c2} value of 6.7 T ($H\|c$) at a reduced temperature $t = (T/T_c(0))$ of 0.14. The $LuNi_2B_2C$ crystals have transition temperatures near 16.1 K and H_{c2} value of 6.4 T ($H\|c$) at reduced temperature $t = (T/T_c(0))$ of 0.13. Both $LuNi_2B_2C$ and YNi_2B_2C have the $ThCr_2Si_2$-type tetragonal structure (I4/mmm), with stacks of alternating rock salt Lu(Y)C and Ni_2B_2 layers [14]. DC magnetisation measurements were performed using a 12 T vibrating sample magnetometer (Oxford Instruments, UK) and a 7.5 T SQUID magnetometer (MPMS7 Quantum Design Inc., USA). The AC susceptibility measurements were done on a home-built AC susceptometer [31] with an AC magnetic field (h_{AC}) parallel to the applied DC magnetic field (H). The amplitude of the AC field was chosen to be 0.1 mT (rms) and the frequency was 211 Hz.

3. Results and discussions

3.1 *YNi_2B_2C*

3.1.1 *AC Susceptibility measurements*

Figure 1 shows the plots of temperature variation of (normalised) in-phase AC susceptibility $\chi'(T)$ at different values of the applied DC field ($H\|c$) in the YNi_2B_2C crystal. In the case of zero applied field, one can see a sharp drop in the $\chi'(T)$ response in a featureless manner across the normal superconducting transition. $\chi'(0)$ curve provides a measure of the width of the normal to superconducting transition in the given crystal. Recalling that, $\chi' \sim = -1 + \alpha h_{AC}/J_c$, where α is a geometry and size dependent factor [32], the presence of an anomalous dip in $\chi'(T)$ curves obtained for $\mu_0 H \geq 0.5$ T corresponds to the occurrence of the peak effect (PE) in $J_c(T)$ at a given H. Note that the PE is a sharp transition in $\mu_0 H = 0.5$ T; it

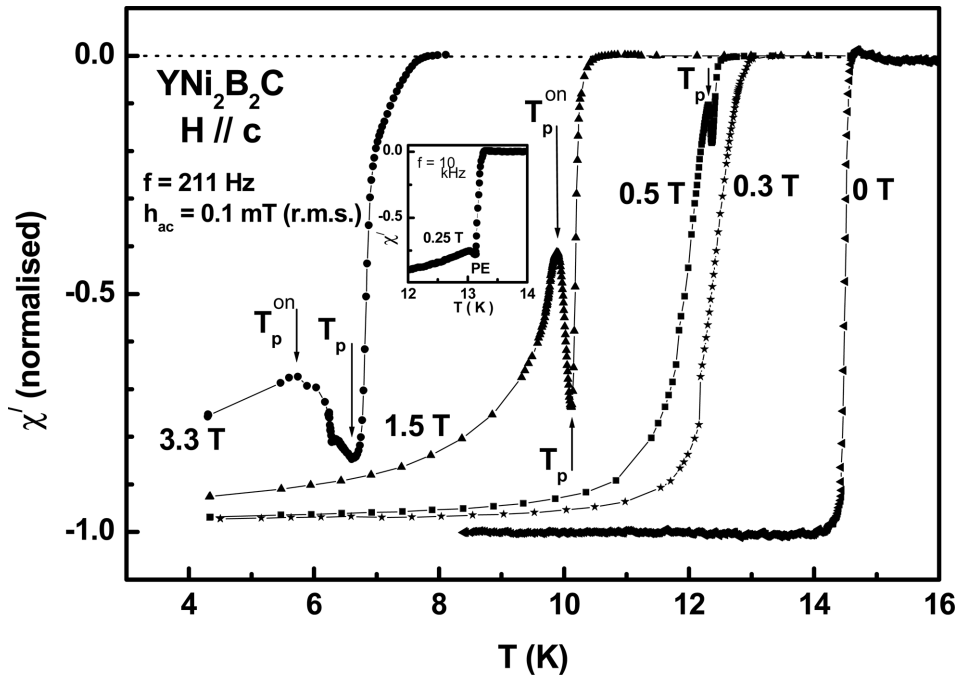

Figure 1. AC Susceptibility ($f = 211$ Hz, $h_{\rm AC} = 0.1$ mT (rms)) data at the DC fields indicated in a single crystal of YNi_2B_2C for $H\|c$. The inset panel shows AC susceptibility at a frequency of 10 kHz at $\mu_0 H = 0.25$ T ($\|c$) in the same crystal. The onset ($T_{\rm p}^{\rm on}$) and peak temperatures ($T_{\rm p}$) of the PE have been marked.

compares favourably with the width of the superconducting transition in zero field. As the applied field increases, the PE transition first broadens (see the curve at $\mu_0 H = 1.5$ T). This is followed by the appearance of multiple step-like features (see curve at $\mu_0 H = 3.3$ T) characterising the phenomenon of step-wise fracturing of the ordered flux-line lattice, consistent with the behaviour well-documented in the context of typically weakly pinned crystals of several low-temperature superconductors [33,34] and a crystal of high $T_{\rm c}$ system, viz., $YBa_2Cu_3O_7$ [35]. At $\mu_0 H < 0.5$ T, the PE dip becomes progressively shallower and for $\mu_0 H = 0.3$ T, the anomalous dip in χ' is not discernible in the χ' measurement made at a frequency of 211 Hz. The non-observation of the PE at low fields is considered to imply that flux line lattice is not very well-formed for intervortex spacing, a_0, larger than the penetration depth λ, which is roughly the distance over which the vortices interact effectively. The intervortex spacing at $\mu_0 H = 0.5$ T for the square FLL symmetry is $\sim$70 nm, comparable to the penetration depth value in the YNi_2B_2C system [20,36]. However, it is known that the state of the FLL order in a given weakly pinned superconductor can be improved by external driving forces. This fact is amply illustrated by the $\chi'(T)$ curve in the inset panel of figure 1, which was obtained in $\mu_0 H = 0.25$ T at a frequency of 10 kHz. One can notice the presence of the PE dip in the inset panel, implying the occurrence of an order–disorder transition for the vortex

state at $\mu_0 H = 0.25$ T, and when measurements are made at a higher frequency of 10 kHz.

The oscillatory field $h_{\rm AC}$ performs a dual role: it not only invokes macroscopic currents in the sample but, also, assumes the role of reorganising the underlying vortex state by facilitating the metastable pinned vortex bundles to transform towards their stationary configurations at a given H/T. The PE imbibes characteristics of a complex dynamical transition. $\chi'(T)$ measurements at different frequencies (in the range of 100 Hz to 0.1 Hz) in a very weakly pinned (nascent) specimen of 2H-$NbSe_2$ had revealed [37] that the anomalous dip in $\chi'(T)$ response becomes less and less conspicuous as the frequency progressively decreases. A comparison of data at 0.3 T in the main panel of figure 1 with that in the inset panel at $\mu_0 H = 0.25$ T appears to echo the earlier observations in a 2H-$NbSe_2$ crystal [37].

Banerjee *et al* [38] had performed a systematic study of the effect of disorder on the shape and magnitude of the PE using crystals of 2H-$NbSe_2$ as their model system. They observed that with the progressive increase in the amount of quenched random disorder present in the 2H-$NbSe_2$ crystals, the PE evolves from being a very narrow transition (for the nascent pinned samples) to a broader transition (for more stronger pinned samples). Comparing this scenario with the plots shown in figure 1, where the PE becomes broader as the applied field is increased, we can surmise that the increase in the applied field plays an equivalent role of an enhancement in the effective disorder.

3.1.2 *Magnetisation hysteresis measurements*

The panel (a) of figure 2 shows a portion of the magnetisation hysteresis (M vs. H) plot in the YNi_2B_2C crystal for $H \| c$ at a temperature of 2.5 K recorded using a VSM with a field ramp rate of 0.3 T/min. The PE bubble can be clearly seen in this panel. The positions of the onset field of the PE, $H_{\rm p}^{\rm on}$, the peak field, $H_{\rm p}$, as well as the upper critical field, H_{c2}, have been marked. One can also notice the presence of a SMP anomaly deep inside the mixed state. The maximum field of the SMP anomaly, $H_{\rm smp}$, is marked. The observation of a SMP anomaly distinct from the PE anomaly in an isothermal M–H scan in YNi_2B_2C is analogous to the behaviour reported in the samples of a few low-temperature superconductors, like, $Ca_3Rh_4Sn_{13}$ [9] and $NbSe_2$ [39] and a high $T_{\rm c}$ compound, $YBa_2Cu_3O_7$ [10,11].

The panel (b) of figure 2 shows the plots of (normalised) $J_{\rm c}$ vs. H at $T =$ 2.5 K and 6.5 K. The $H_{\rm smp}$ and $H_{\rm p}$ values are marked in this panel. It should be noticed that with the increase of temperature, the peak field $H_{\rm p}$ decreases from 5.35 T at $T = 2.5$ K to 3.7 T at $T = 6.5$ K, but the region of SMP anomaly does not seem to show any variation. This implies that $H_{\rm smp}(T)$ varies weakly with temperature. It is also useful to note that the width as well as the height of the PE anomaly enhances as the temperature decreases. This trend is consistent with what is evident from the temperature dependent AC susceptibility data in fields up to $\mu_0 H = 3.3$ T in figure 1. The SMP anomaly of the M–H data does not get fingerprinted in the $\chi'(T)$ scans as the $H_{\rm smp}(T)$ values are nearly temperature independent.

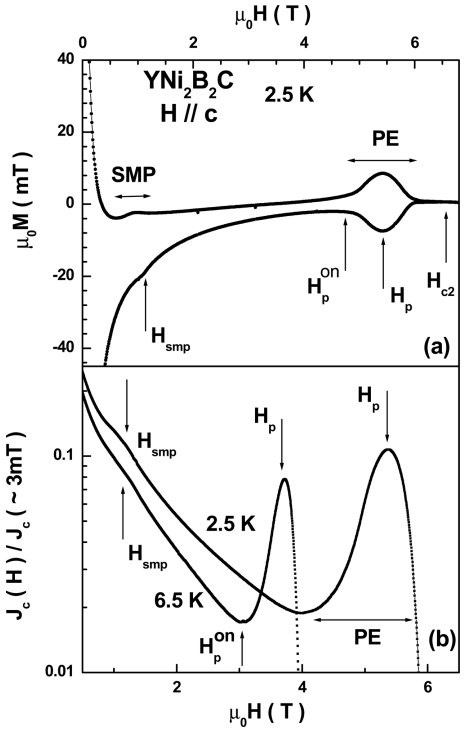

Figure 2. Panel (a) shows a portion of the M–H loop at 2.5 K in the YNi_2B_2C crystal for $H\|c$. The second magnetisation peak anomaly and the peak effect phenomenon can be clearly recognised. The onset (H_p^{on}) and the peak field of the PE and the representative field value of the SMP anomaly have been identified. Panel (b) depicts log-linear plots of the normalised critical current density $J_c(H)/J_c$ (3 mT) (=$\Delta M(H)/\Delta M$ (3mT)) vs. field (H) in YNi_2B_2C crystal for $H\|c$ at 2.5 K and 6.5 K, respectively.

3.1.3 *Flux jumps and the change in local symmetry of the flux line lattice*

Figure 3 shows a complete M–H hysteresis loop recorded with $\mu_0|H_{\max}| = 0.3$ T in the single crystal of YNi_2B_2C for $H\|c$ at 2.1 K using a SQUID magnetometer. Similar loops on the same crystal had been recorded using a VSM earlier [39].

One can straightaway notice the presence of flux jumps in the magnetisation data at certain field values. Two other observations are also self-evident:

(i) In the first quadrant, i.e., the virgin run ($0 \rightarrow \mu_0 H_{\max}$), the second quadrant ($\mu_0 H_{\max} \rightarrow 0$) and the fourth quadrant ($-\mu_0 H_{\max} \rightarrow 0$), there are no sudden changes in the magnetisation values. The flux jumps happen only in the third ($0 \rightarrow -\mu_0 H_{\max}$) and the fifth quadrant (0 to $\mu_0 H_{max}$, in the second cycle).

(ii) The flux jumps in the third quadrant are evident at about −34, −78, −106 and −145 mT, while those in the fifth quadrant appear to happen near field values 78, 114 and 150 mT.

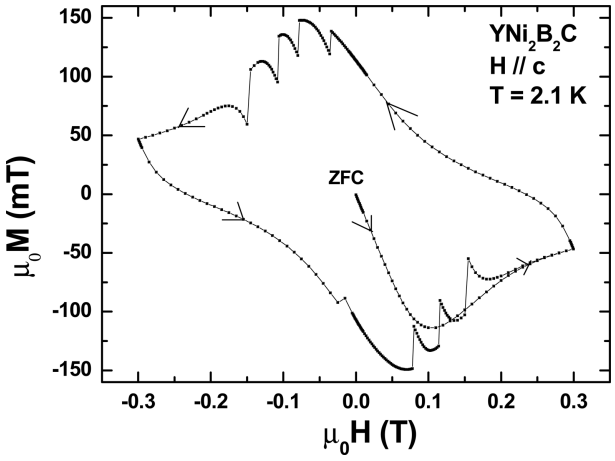

Figure 3. M–H loop obtained by cycling the field between $\mu_0|H_{\max}| = 0.3$ T in the crystal of YNi_2B_2C for $H\|c$ at 2.1 K. The occurrence of sudden (flux) jumps in the magnetisation values can be noted.

We may note that the penetration field in the given sample of YNi_2B_2C crystal for $H\|c$ is estimated to be about 150 mT at 2.1 K (figure 3). We repeated the above experiment several times, changing the thermomagnetic history of the sample, and always found that the flux jumps (their numbers varying between two and four) occurred only in the third and the fifth quadrant. Also, the field values corresponding to the jumps varied up to 10% from the values presented in figure 3. From SANS measurements performed on YNi_2B_2C single crystals [21,22] in the field-cooled states (for $H\|c$), it was found that the flux line lattice in this system undergoes novel structural transitions at low fields. The FLL symmetry underwent a field-induced transition from a nearly hexagonal (rhombohedral) of apex angle β_1 to another hexagonal (rhombohedral) of apex angle β_2 via a 45° re-orientation transition. This happens via a sudden first-order transition at a field H_1. This nearly hexagonal lattice eventually gets transformed to a square symmetry via a continuous transition at a field H_2. We are tempted to ascribe the flux jumps in the magnetisation to the first order 45° re-orientation of the flux line lattice. The observation that flux jumps happen in the third and fifth quadrant implies that the co-existence of domains with opposite sign of local field facilitates the occurrence of these jumps.

It could be difficult to capture the continuous transition (occurring at H_2) via flux jumps. When the effective disorder is high and the field in the sample is non-uniform, the vortex matter in the sample could be considered to comprise many domains within which the quasi-long range order may survive. The average field over these domains (locally) would be expected to be different in a magnetisation hysteresis measurement. Varying number of jumps (from two to four) suggests that the different domains probably reach the H_1 field (locally) at different values of the external applied field.

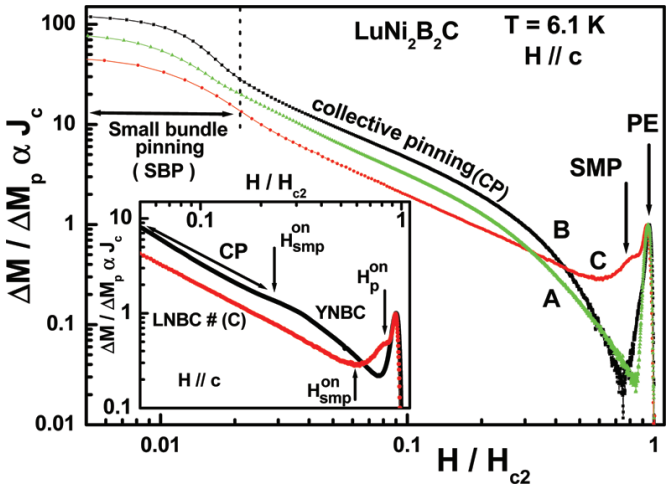

Figure 4. The main panel shows log–log plots of the normalised critical current density vs. normalised field (H/H_{c2}) in the three crystals of $LuNi_2B_2C$ at 6.1 K and for $H\|c$. The PE phenomenon in crystals A and B and the occurrence of a SMP anomaly prior to the PE in crystal C can be easily identified. The field regions of the small bundle pinning (SBP) and the collective pinning (CP) have been indicated. The inset panel shows a comparison of the normalised current density vs. normalised field (H/H_p) in the crystal C of $LuNi_2B_2C$ (at 6.1 K) with that in the crystal of YNi_2B_2C (at 6.5 K) for $H\|c$. Both the crystals display SMP anomaly distinct from the PE anomaly.

3.2 *$LuNi_2B_2C$*

3.2.1 *Magnetisation hysteresis measurements in different crystals*

Figure 4 shows a log–log plot of (normalised) J_c with H/H_{c2} at $T = 6.1$ K in three samples of $LuNi_2B_2C$ extracted from their isothermal magnetisation hysteresis curves. Each sample has different amount of quenched random disorder. Based on these differences, the samples have been designated as A, B and C, with A being the most weakly pinned. All the three crystals appear to display similar $J_c(h)$ response at very low fields and in the field region up to about 2 T. Above about 2 T, the sample C displays SMP anomaly followed by the PE phenomenon. On the other hand, in crystals A and B, one witnesses only the PE anomaly. The peak in $J_c(h)$ at 6.1 K is sharper in crystal A than that in crystal B. The ratio of the critical current density at the peak position to that at the onset position of the PE is approximately the same (≈30) in crystals A and B. The ratio of about thirty implies that the radial and longitudinal correlation lengths prior to the onset of the PE shrink to about one tenth of their sizes while reaching the peak position. Figure 4 also shows that in crystal C, J_c enhances by a factor of about three from the onset position of the SMP anomaly to the peak position of PE in two steps.

The log–log plots as displayed in figure 4 are often used to demarcate the various regimes of pinning [40]. When the intervortex separation, a_0, is greater than

the penetration depth λ, the flux lines interact very weakly, since λ is the length scale over which repulsive interaction between vortices decays. As a result, at very low fields each flux line can get individually pinned and the macroscopic current density in such a circumstance is very weakly dependent on the field. This is often designated as the small bundle pinning (SBP) regime (figure 4). In figure 4, we have notionally put the limit of SBP regime at the reduced field (H/H_{c2}) of 0.02 at 6.1 K which corresponds to an a_0 value of nearly 140 nm (which is about twice the λ value reported in $LuNi_2B_2C$ [20,36]). As the applied field increases gradually so that a_0 approaches the λ value, the flux lines start interacting effectively and a cross-over is expected to occur towards the collective pinning regime. The dependence of J_c on H slowly enhances and it progresses to power-law regime, $J_c \propto H^{-n}$. Stronger interactions lead to the formation of a well-ordered FLL with large-sized domains extending over the entire sample. It is widely accepted in the literature that the FLL amorphises above the onset field/temperature of the PE. Intuitively, it seems plausible that the process of amorphisation from the large-sized domains (i.e., a quasi-Bragg glass regime) occurs via two steps. In the first step, the Bragg glass (BG) state gets broken up into small multi-domain (vortex glass) state. In the second step, the multidomain vortex glass state amorphises into microdomains.

The inset panel in figure 4 shows a comparison of (normalised) J_c in crystal C of $LuNi_2B_2C$ at 6.1 K with the corresponding behaviour in the crystal YNi_2B_2C at 6.1 K. Both these samples display the SMP and the PE. However, the SMP anomaly in the latter sample is located deeper inside the mixed phase and is well-separated from the PE. A larger field interval between the SMP and the PE anomalies allows the possibility of partial healing of the dislocations injected at the onset field of the SMP. Note that the ratio of the J_c value at the peak position of the PE to that at the onset field of the PE in YNi_2B_2C is slightly larger than the ratio of the J_c values at the peak position of PE to that at the onset of the SMP in $LuNi_2B_2C$. Both these ratios are, however, smaller than the corresponding values in the samples A and B of $LuNi_2B_2C$, which do not display the SMP anomaly.

Figure 5 shows the plots of J_c vs. H at different temperatures in the crystal A of $LuNi_2B_2C$ for $H \| c$. It is apparent that the PE anomaly manifests in a robust manner at lower temperatures and higher fields. The inset panel in figure 5 displays the plots of (normalised) J_c values ($J_c(H)/J_c(H_p)$) vs. reduced field (H/H_p) at different temperatures.

In figure 6, we have plotted the pinning force density ($\propto$ (normalised) $J_c \times H$) vs. field in the YNi_2B_2C crystal at 2.5 K for $H \| c$. The pinning force curve in figure 6 displays three maxima. The first maximum near 150 mT corresponds to the usual maximum in the pinning force, implying the rigidity of the well-formed flux line lattice. The maximum just before the H_{c2} value fingerprints the peak effect phenomenon triggered by the faster collapse in the elasticity of the FLL *vis-à-vis* the collapse in the pinning force [2]. A small maximum located near $\sim$1.1 T imprints the occurrence of second magnetisation peak anomaly. In the inset panel of figure 6, we show the comparison of the behaviour of the pinning force density vs. reduced field (H/H_p) in the YNi_2B_2C crystal at 6.5 K and 2.5 K. It may also be noted that the flux jumps of figure 3, which presumably correspond to the sudden change in the local symmetry of flux line lattice, also leave their imprint in the pinning force curve at field values below that of the first maximum.

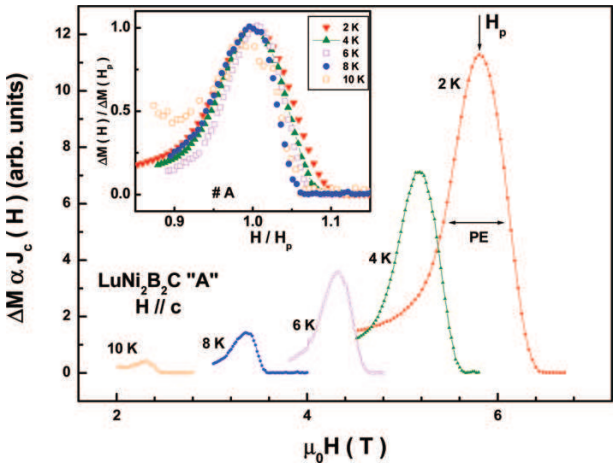

Figure 5. Plots of the critical current density vs. field across the PE region at different temperatures in crystal A of $LuNi_2B_2C$. The inset panel shows the plots of the normalised critical current density ($\propto \Delta M(H)/\Delta M(H_p)$) vs. normalised field ($H/H_p$) at different temperatures.

The observation that different plots overlap in the inset panels of figures 5 and 6 attest to the scaling behaviour operative for the pinning force as regards the PE phenomenon, and this is in conformity with the assertions made by Higgins and Bhattacharya [41] in the context of their data in the 2H-$NbSe_2$ system. The scaling behaviour does not hold for the SMP anomaly (cf. 6.5 K and 2.5 K data in the inset panel of figure 6). We believe that the SMP anomaly is pinning induced, occurs at the same field at 2.5 K and 6.5 K, and therefore, does not scale with the notion of reduced field, i.e., H/H_{c2} (or H/H_p).

It is useful to note in figure 5 that the ratio of J_c at the peak position to that at the onset field is largest for $T = 6$ K and, also, that the PE appears narrowest for $T = 6$ K. Above 8 K and below 4 K, the PE peaks in the inset panel show broadening and the said ratio of J_c also reduces somewhat. Such a trend can be rationalised in terms of the notion of enhancement in effective disorder at the high field end ($\mu_0 H \geq 6$ T, $T \leq 2$ K) and approach towards small bundle pinning regime at the low field end ($\mu_0 H < 0.5$ T, $T > 12$ K).

3.2.2 *Flux jumps in crystal C of $LuNi_2B_2C$*

The panel (a) of figure 7 shows a portion of the M–H plot in the so-called fifth quadrant ($0 \rightarrow 0.03$ T second sequence) on an expanded scale in sample C of $LuNi_2B_2C$ for $H \| c$. The M–H loop was recorded using a VSM at a ramp rate of 0.25 mT/min with $\mu_0|H_{max}| = 0.03$ T. Similar to the flux jumps seen in YNi_2B_2C (figure 3), one can notice the occurrence of flux jumps in this $LuNi_2B_2C$ sample (#C). In panel (a) of figure 7, there are three flux jumps at 10 mT, 15 mT and 22 mT.

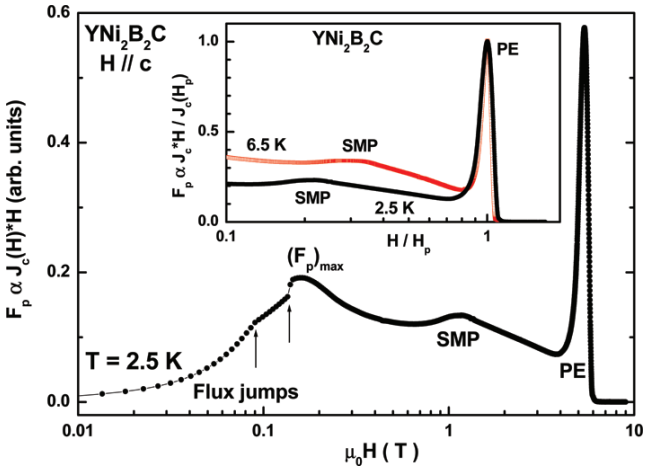

Figure 6. Plot of the pinning force density ($\propto$ normalised $J_c \times H$) vs. field in a crystal of YNi_2B_2C at 2.5 K. $(F_p)_{max}$, SMP and PE have been demarcated. Also note the flux jumps before $(F_p)_{max}$. The inset panel shows the normalised pinning force density ($\propto$ normalised $J_c \times H/J_c(H_p)$ vs. normalised field (H/H_p) at 2.5 K and 6.5 K.

Panel (b) of figure 7 shows a portion of the M–H plot in $LuNi_2B_2C$ (#C) in the negative field direction ($0 \rightarrow -0.03$ T) at the same temperature and for $H \| c$. In this plot also, one can notice jumps in the magnetisation values at -23 mT, -15 mT and -10 mT.

The field values of the flux jumps in panels (a) and (b) of figure 7 are of the same order as the H_1 field values in $LuNi_2B_2C$ (between 20 to 50 mT), where the FLL undergoes a first-order transition from the rhombohedral R_1 to the rhombohedral R_2 via a 45° re-orientation [24].

3.2.3 *Temperature dependence of the upper critical fields in sample A of $LuNi_2B_2C$*

The magnetisation curves in all the three crystals of $LuNi_2B_2C$ start to show oscillations before the arrival of the PE region. These oscillations continue across into the normal region, where they manifest in a spectacular manner revealing their identity as the dHvA oscillations. The dHvA oscillations have been recorded in crystals A and B from 0.1 to 15 K for $H \| c$ and from 0.1 to 6 K for $H \| ab$. In the presence of dHvA oscillations, the identification of H_{c2} becomes ambiguous. To overcome this difficulty, we had resorted to the option of preferentially recording the quadrupolar signal (**Q**) using vibrating sample magnetometer and determined $H_{c2}(T)$ values for $H \| c$ and $H \| ab$ [42].

Figure 8 displays a plot of H_{c2} vs. reduced temperature $(T/T_c(0))$ for $H \| c$ and $H \| ab$ in crystal A of $LuNi_2B_2C$. The inset panel in figure 8 shows that near $T_c(0)$, $H_{c2}(t)$ curve has a positive curvature which crosses over to the usual negative curvature as t reduces below 0.95. An attempt to conform the observed curvature

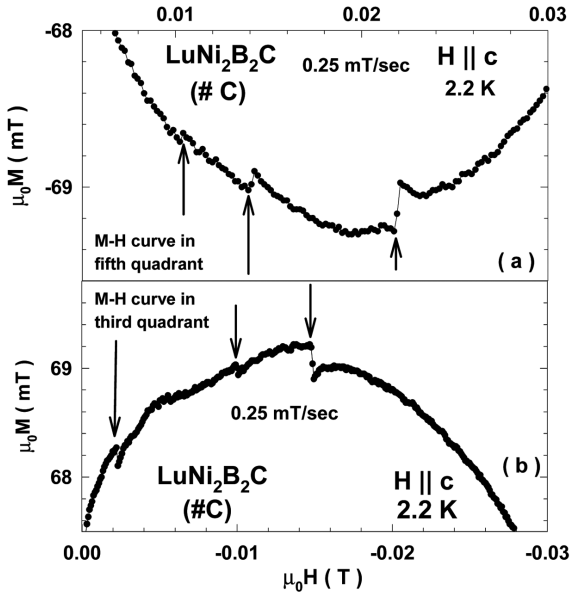

Figure 7. Expanded views of the portions of M–H curves obtained in crystal C of $LuNi_2B_2C$ at 2.1 K, while cycling between $\mu_0|H_{\max}| = 0.3$ T. The panel (a) depicts the curve in the fifth quadrant (i.e., ramping field up from 0 to $\mu_0 H_{\max} = 0.3$ T) and the panel (b) shows the data obtained in the third quadrant (i.e., ramping field down from 0 to $\mu_0 H_{\min} = -0.3$ T).

of the $H_{c2}(t)$ data points to the Ginzburg–Landau (GL) theory while including the non-local corrections [43] did not give a very good fit. We, therefore, resorted to fitting the observed $H_{c2}(t)$ data points to an isotropic s-wave two band Ginzburg–Landau model [44]. The solid lines passing through data points in figure 8 represent fitting to the two-band model, with two different order parameters corresponding to each band. Having written the total free energy as the sum of the free energies from each band and considering an interband scattering term, two G–L equations are obtained by minimising the total free energy. From the fitting, the zero temperature value of H_{c2} for $H\|ab$ and $H\|c$ were determined to be 8.2 T and 6.5 T, respectively. These values incidentally are very close to the value measured (6.8 T for $H\|c$ and 8.2 T for $H\|ab$) at 100 mK for $H\|c$ and $H\|ab$, while performing the dHvA measurements in the same crystal (data not shown here).

The anisotropy ratio, $H_{c2}(0)_{H\|ab}/H_{c2}(0)_{H\|c} = 1.21$ is consistent with the value reported in the literature from an analysis of the data at 3 K [42,43]. A close look into the inset panel of figure 8 reveals that the fitting to the data points above $t = 0.85$ still leaves some discrepancy for $H\|c$. A possible explanation for this discrepancy could be that the fitting has been done assuming only two bands but there are recent experiments which suggest these compounds to have more than two bands (multibands) [45] contributing to superconductivity.

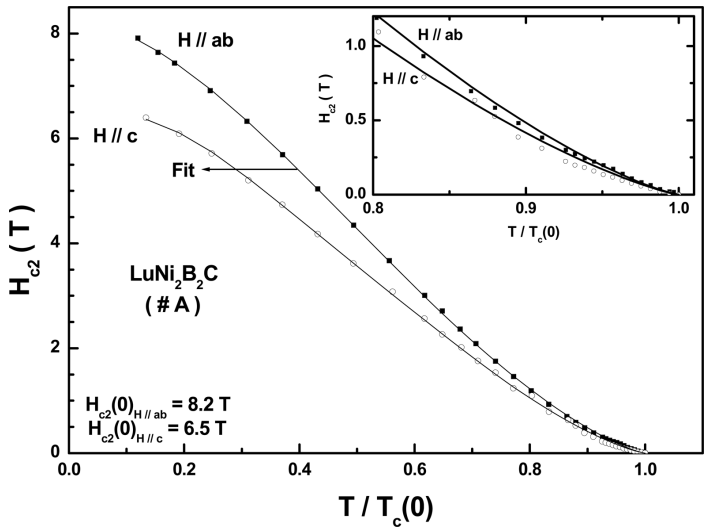

Figure 8. Plots of the upper critical field vs. reduced temperature in crystal A of $LuNi_2B_2C$ for $H\|c$ as well as $H\|ab$. The solid lines are fits to the data using the framework of isotropic s-wave two-band Ginzburg–Landau model. The values of $H_{c2}(0)$ obtained in the two cases are indicated in this panel. The inset panel shows the discrepancy between the fitted curves and the data points on an expanded scale.

3.3 *Vortex phase diagram in YNi_2B_2C for $H\|c$*

Figure 9 shows a sketch of the vortex phase diagram in a crystal of YNi_2B_2C for $H\|c$ by collating all the temperatures and field values at which some typical as well as anomalous features could be noted in the AC susceptibility as well as magnetisation hysteresis measurements.

In figure 9, H_{c2}/T_c, H_p^{on}/T_p^{on}, H_{smp}^{on}, H_{sbp} (limit of small bundle pinning) and H_{c1} lines have been shown. Between H_{c1} and H_{c2}, the mixed state can be subdivided into different regions.

Between H_{c1} and H_{sbp} (the limiting field for the small bundle pinning regime), the vortex matter is divided into small domains where the flux line lattice gets pinned collectively. The resultant state is only partially ordered. The flux line lattice symmetry in different domains in this regime could be locally different [24,46]. SANS and Bitter decoration images obtained at low fields (<100 mT) in crystals of YNi_2B_2C and $LuNi_2B_2C$ respectively for $H\|c$ would tend to support this scenario. At fields below H_{sbp}, the temperature scans do not yield PE in χ'_{AC} measurements. Between H_{sbp} and the onset field of the second magnetisation peak, i.e., H_{smp}^{on}, the order in the vortex state improves and the lattice presumably comprises very large sized domains (a quasi-Bragg glass state) having square symmetry for FLL. The PE peak in $\chi'_{AC}(T)$ scans is sharp for $H_{sbp} < H < H_{smp}^{on}$. It can be noticed that the H_{smp}^{on} line is nearly flat exhibiting a behaviour reminiscent of the H_{smp}^{on} line reported in another weakly pinned superconductor, viz., $Ca_3Rh_4Sn_{13}$ [9]. In such circumstances, the H_{smp}^{on} line does not get fingerprinted in $\chi'_{AC}(T)$ scans. This

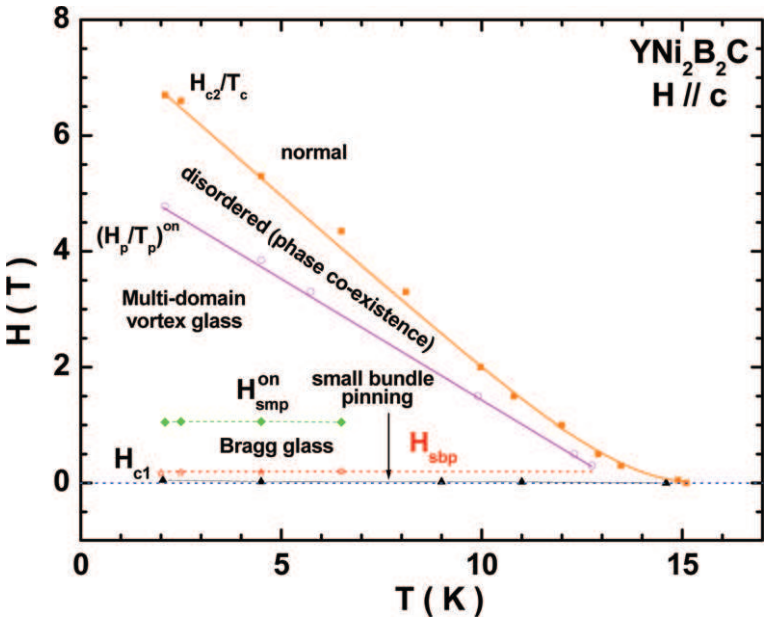

Figure 9. A sketch of the vortex phase diagram in the crystal of YNi_2B_2C for $H\|c$. Various phases of the vortex solid, viz., small bundle pinning, Bragg glass, multidomain vortex glass and disordered phase of co-existing ordered and disordered solid have been demarcated. Also one can notice the positive curvature in $H_{c2}(T)$ near $T_c(0)$.

behaviour is different from the behaviour of H^{on}_{smp} line in crystals of 2H-$NbSe_2$ [47], where the shape of the line is such that SMP anomaly could be detected both in isofield as well as isothermal AC susceptibility scans.

As stated earlier, the SMP anomaly probably marks the transition from a quasi-Bragg glass state to a multi-domain vortex glass phase. It is tempting to relate the H_{smp} value of 1 T to the reported reduction in the transverse correlation length at a similar field value in the crystals of YNi_2B_2C and $LuNi_2B_2C$ for $H\|c$ via a SANS study earlier [20]. For field values between H^{on}_{smp} and H^{on}_{p}, $\chi'_{AC}(T)$ scans reveal a broadened PE, with a notion of fracturing evident at some field values (e.g. $\chi'_{AC}(T)$ curve at 3.3 T in figure 1).

Above H^{on}_{p}, the vortex solid gets broken up into micro-domains and it progresses towards the completely amorphous state on going across the peak field values. This disordered region above H^{on}_{p} appears to also extend to the small bundle pinning regime at the low field end. The closer approach of the H_{sbp} line and the H^{on}_{p} line near $T_c(0)$ end gives it the notion of a 'nose feature' frequently sketched in the phase diagrams drawn for 2H-$NbSe_2$ crystals [40,47–49]. In the 2H-$NbSe_2$ crystals, the PE region is considered to comprise the phase co-existence regime of ordered and disordered regions [50]. In this spirit, we have demarcated the phase space above the H^{on}_{p} line as the phase co-existence region.

Note also the shape of the H_{c2} line in figure 9. It again shows the positive curvature in the low field and high temperature part of the phase diagram, similar to

the behaviour shown in $LuNi_2B_2C$ (see figure 8). This suggests that both $LuNi_2B_2C$ and YNi_2B_2C are possible candidates for multiband superconductivity.

4. Conclusions

In conclusion, we have explored the vortex state in the crystals of two non-magnetic borocarbide superconductors, viz., YNi_2B_2C and $LuNi_2B_2C$ via the magnetisation measurements. Structural transitions in the FLL at low fields seem to leave an imprint in the M–H loops via the flux jumps in the weakly pinned crystals of both YNi_2B_2C and $LuNi_2B_2C$, while the (spatial) order–disorder transformations get captured via anomalous variations in the critical current density. Taking crystals of $LuNi_2B_2C$ as an example, we have tried to show that the SMP anomaly in the vortex solid is pinning induced and it is a characteristic feature of weakly pinned superconductors. Finally, we have sketched the vortex phase diagram in a crystal of YNi_2B_2C for $H \| c$ which shows the SMP anomaly and the PE.

Acknowledgments

Two of us (DJ-N and DP) would like to thank the TIFR Endowment Fund for partial financial support in the form of Kanwal Rekhi career development award.

References

[1] T G Berlincourt, R R Hake and D H Leslie, *Phys. Rev. Lett.* **6**, 671 (1961)
[2] A B Pippard, *Philos. Mag.* **19**, 217 (1969)
[3] A I Larkin and Y N Ovchinnikov, *Sov. Phys. JETP* **38**, 854 (1974)
[4] A I Larkin, *Sov. Phys. JETP* **31**, 784 (1974)
[5] A I Larkin and Yu N Ovchinnikov, *J. Low Temp. Phys.* **34**, 409 (1979)
[6] M Daeumling, J M Seuntjens and D C Larbalestier, *Nature (London)* **346**, 332 (1990)
[7] N Chikumoto, M Konczykowski, N Motohira and A P Malozemoff, *Phys. Rev. Lett.* **69**, 1260 (1992)
[8] B Khaykovich, E Zeldov, D Majer, T W Li, P H Kes and M Konczykowski, *Phys. Rev. Lett.* **76**, 2555 (1996)
[9] S Sarkar, P L Paulose, S Ramakrishnan, A K Grover, C V Tomy, G Balakrishnan and D McK Paul, *Physica* **C356**, 181 (2001)
[10] D Pal, S Ramakrishnan, A K Grover, D Dasgupta and B K Sarma, *Phys. Rev.* **B63**, 132505 (2000)
[11] D Pal, S Ramakrishnan and A K Grover, *Phys. Rev.* **B65**, 096502 (2001)
[12] S Sarkar, D Pal, P L Paulose, S Ramakrishnan, A K Grover, C V Tomy, D Dasgupta, Bimal K Sarma, G Balakrishnan and D McK Paul, *Phys. Rev.* **B64**, 144510 (2001)
[13] R Nagarajan, Chandan Mazumdar, Zakir Hossain, S K Dhar, K V Gopalakrishnan, L C Gupta, C Godart, B D Padalia and R Vijayaraghavan, *Phys. Rev. Lett.* **72**, 274 (1994)
[14] R J Cava, H Takagi, H W Zandbergen, J J Krajewski, W F Peck, T Siegrist, B Batlogg, R B van Dover, R J Felder, K Mizuhashi, J O Lee, H Eisaki and S Uchida, *Nature (London)* **367**, 252 (1994)

[15] P C Canfield, P L Gammel and D J Bishop, *Phys. Today* **51(10)**, 40 (1998) and references therein
[16] H Eisaki, H Takagi, R J Cava, B Batlogg, J J Krajewski, W F Peck, K Mizuhashi, J O Lee and S Uchida, *Phys. Rev.* **B50**, 647 (1994)
[17] J W Lynn, S Skanthakumar, Q Huan, S K Sinha, Z Hossain, L C Gupta, R Nagarajan and C Godart, *Phys. Rev.* **B55**, 6584 (1997)
[18] P Raychaudhuri, D Jaiswal-Nagar, G Sheet, S Ramakrishnan and H Takeya, *Phys. Rev. Lett.* **93**, 156802 (2004)
[19] K Izawa, K Kamata, Y Nakajima, Y Matsuda, T Watanabe, M Nohara, H Takagi, P Thalmeier and K Maki, *Phys. Rev. Lett.* **89**, 137006 (2002)
[20] M R Eskildsen, P L Gammel, B P Barber, A P Ramirez, D J Bishop, N H Andersen, K Mortensen, C A Bolle, C M Lieber and P C Canfield, *Phys. Rev. Lett.* **79**, 487 (1997)
[21] D Mck Paul, C V Tomy, C M Aegerter, R Cubitt, S H Lloyd, E M Forgan, S L Lee and M Yethiraj, *Phys. Rev. Lett.* **80**, 1517 (1998)
[22] C D Dewhurst, S J Levett and D McK Paul, *Phys. Rev.* **B72**, 014542 (2005)
[23] L Ya Vinnikov, T L Barkov, P C Canfield, S L Bud'ko and V G Kogan, *Phys. Rev.* **B64**, 024504 (2001)
[24] L Ya Vinnikov, T L Barkov, P C Canfield, S L Bud'ko, J E Ostenson, F D Laabs and V G Kogan, *Phys. Rev.* **B64**, 220508 (2001)
[25] K Hirata, H Takeya, T Mochiku and K Kadowaki, in: *Proceedings of the 8th Int. Symp. Superconductivity* edited by H Hayakawa and Y Enomoto (Springer-Verlag, Tokyo, 1996) p. 619
[26] K J Song, J R Thompson, M Yethiraj, D K Christen, C V Tomy and D McK Paul, *Phys. Rev.* **B59**, R6620 (1999)
[27] S S James, C D Dewhurst, R A Doyle, D McK Paul, Y Paltiel, E Zeldov and A M Campbell, *Physica* **C332**, 173 (2000)
[28] V G Kogan, M Bullock, B Harmon, P Miranovic, Lj Dobrosavljevic Grujic, P L Gammel and D J Bishop, *Phys. Rev.* **B55**, R8693 (1997)
[29] Ming Xu, P C Canfield, J E Ostenson, D K Finnemore, B K Cho, Z R Wang and D C Johnston, *Physica* **C227**, 321 (1994)
[30] H Takeya, T Hirano and K Kadowaki, *Physica* **C256**, 220 (1996)
[31] S Ramakrishnan, S Sundaram, R S Pandit and G Chandra, *J. Phys.* **E18**, 650 (1985)
[32] X S Ling and J I Budnick, in: *Magnetic susceptibility of superconductors and other spin systems* edited by R A Hein, T L Francavilla and D H Leibenberg (Plenum Press, New York, 1991) p. 377
[33] S Sarkar, D Pal, S S Banerjee, S Ramakrishnan, A K Grover, C V Tomy, G Ravikumar, P K Mishra, V C Sahni, G Balakrishnan, D McK Paul and S Bhattacharya, *Phys. Rev.* **B61**, 12394 (2000)
[34] S S Banerjee, N G Patil, S Saha, S Ramakrishnan, A K Grover, S Bhattacharya, G Ravikumar, P K Mishra, T V Chandrasekhar Rao, V C Sahni, M J Higgins, E Yamamoto, Y Haga, M Hedo, Y Inada and Y Onuki, *Phys. Rev.* **B58**, 995 (1998)
[35] D Pal, D Dasgupta, Bimal K Sarma, S Bhattacharya, S Ramakrishnan and A K Grover, *Phys. Rev.* B**62**, 6699 (2000)
[36] M Yethiraj, D McK Paul, C V Tomy and E M Forgan, *Phys. Rev. Lett.* **78**, 4849 (1997)
[37] C V Tomy, D Pal, S S Banerjee, S Ramakrishnan, A K Grover, S Bhattacharya, M J Higgins, G Balakrishnan and D McK Paul, *Pramana – J. Phys.* **58**, 925 (2002)

[38] S S Banerjee, N G Patil, S Ramakrishnan, A K Grover, S Bhattacharya, P K Mishra, G Ravikumar, T V Chandrasekhar Rao, V C Sahni, M J Higgins, C V Tomy, G Balakrishnan and D Mck Paul, *Phys. Rev.* **B59**, 6043 (1999)
[39] D Pal, *Magnetic phase diagram in Type II superconductors*, Ph.D. Thesis (University of Mumbai, Mumbai, 2002)
[40] S S Banerjee, S Ramakrishnan, A K Grover, G Ravikumar, P K Mishra, V C Sahni, C V Tomy, G Balakrishnan, D McK Paul, P L Gammel, D J Bishop, E Bucher, M J Higgins and S Bhattacharya, *Phys. Rev.* **B62**, 11838 (2000)
[41] M J Higgins and S Bhattacharya, *Physica* **C257**, 232 (1996)
[42] D Jaiswal-Nagar, A D Thakur, M R Eskildsen, P C Canfield, S M Yusuf, S Ramakrishnan and A K Grover, *Physica* **B359–361**, 476 (2005)
[43] V Metlushko, U Welp, A Koshelev, I Aranson, G W Crabtree and P C Canfield, *Phys. Rev. Lett.* **79**, 1738 (1997)
[44] I N Askerzade, *Physica* **C397**, 99 (2003)
[45] S Mukhopadhyay, G Sheet, P Raychaudhuri and H Takeya, *Phys. Rev.* **B72**, 014545 (2005)
[46] S J Levett, C D Dewhurst and D McK Paul, *Phys. Rev.* **B66**, 014515 (2002)
[47] A D Thakur, S S Banerjee, M J Higgins, S Ramakrishnan and A K Grover, *Phys. Rev.* **B72**, 134524 (2005), cond-mat/0509514
[48] Y Paltiel, E Zeldov, Y Myasoedov, M L Rappaport, G Jung, S Bhattacharya, M J Higgins, Z L Xiao, E Y Andrei, P L Gammel and D J Bishop, *Phys. Rev. Lett.* **85**, 3712 (2000)
[49] A D Thakur, S S Banerjee, M J Higgins, S Ramakrishnan and A K Grover, *Pramana – J. Phys.* **66**, 159 (2006)
[50] M Marchevsky, M J Higgins and S Bhattacharya, *Nature (London)* **409**, 591 (2001)